21st Australasian Fluid Mechanics Conference
Adelaide, Australia
10-13 December 2018

Artificial intelligence control of a turbulent jet

Dewei Fan[1,2], Yu Zhou[1,2], Bernd R. Noack[1,3,4]
[1]Institute for Turbulence-Noise-Vibration Interaction and Control,
Harbin Institute of Technology, Shenzhen, China
[2]Digital Engineering Laboratory of Offshore Equipment, Shenzhen, China
[3]Laboratoire d'Informatique pour la Mécanique et les Sciences de l'Ingénieur, LIMSI-CNRS, Rue John von Neumann, Campus Universitaire d'Orsay, Bât 508, F-91403 Orsay Cedex, France
[4]Institut für Strömungsmechanik und Technische Akustik (ISTA)
Technische Universität Berlin, Müller-Breslau-Straβe 8, D-10623 Berlin, Germany

Abstract

An artificial intelligence (AI) control system is developed to manipulate a turbulent jet with a view to maximizing its mixing. The system consists of sensors (two hot-wires), genetic programming for learning/ evolving and execution mechanism (6 unsteady radial minijets). Mixing performance is quantified by the jet centerline mean velocity. AI control discovers a hitherto unexplored combination of flapping and helical forcings. Such a combination of several actuation mechanisms—if not creating new ones—is practically inaccessible to conventional methods like a systematic parametric analysis and gradient search, and vastly outperforms the optimized periodic axisymmetric, helical or flapping forcing produced from conventional open- or closed-loop controls. Intriguingly, the learning process of AI control discovers all these forcings in the order of increased performance. The AI control has dismissed sensor feedback and multi-frequency components for optimization. Our study is the first highly successful AI control experiment for a non-trivial spatially distributed actuation of a turbulent flow. The results show the great potential of AI in conquering the vast opportunity space of control laws for many actuators and sensors and manipulating turbulence.

Introduction

Our experimental study builds on the pioneering numerical jet mixing studies ([5, 6]). The former deployed an evolutionary strategy to optimize a combination of axisymmetric and helical forcing characterized by four parameters, while the latter optimized a flapping mode [10]. The present optimization method, based on linear genetic programming (LGP), may work on a much larger search space of spatio-temporal forcing including all known three-dimensional actuations, multi-frequency forcing and sensor feedback.

In general, active control of jets is divided into open-loop and closed-loop control. Note that closed-loop control shows the potential to significantly reduce power requirements in comparison to open-loop control strategies, since the random aspect of these structures reduces the effectiveness of an open-loop configuration [7]. Most literature on closed-loop turbulent flow control falls in two categories, i.e. model-based and model free tuning of the control laws. For model-based control, the discretised Navier-Stokes equations and linear stochastic estimation are used to resolve all flow physics and nonlinearities [11]. In the previous work [1], reduced-order models were applied to a few non-normal global eigenmodes of the linearized Navier- Stokes equations as a basis for Galerkin projection. Yet, these approaches have limited applicability to unstable advection dominated flows [8]. The control logic based on models is the most accurate. However, the accurate control consumes too much time. Therefore, model-free control is most widely applied in the turbulent flow control. The adaptive control PID was used to suppress cylinder vibration [16]. Extremum seeking control (ESC) was used for separation control on a high lift configuration [2]. Yet, in all reported cases the resulting control law was simple, e.g. based on a single actuator characterizable by one or two parameters. The optimization of such control laws is achievable with conventional techniques [13]. The nonlinear control optimization involving many independent actuators can be unimaginably complex. Take the manipulation of a turbulent jet based on unsteady radial minijets for example. One single periodically operated minijet of a given exit diameter may be associated with three control parameters, namely, the excitation frequency f_e, mass flow rate m_{mini} and duty cycle α [9]; however, multiple, say six, equally separated independent minijets introduce the complexity of distributed actuation or additional dimensions. The minijets can be active or off and six minijets may occur alternately from one configuration to the other. As a result, the complexity of the problem grows tremendously. The optimization of nonlinear control laws for such high dimension problems is largely terra incognita, which is extremely too time consuming, if not impossible, for conventional techniques. This is a great challenge for turbulence control. Then could artificial intelligence method conquer the vast opportunity space of control laws and, in doing so, generate an outcome or alter the turbulence to a desired state that has been so far prohibitive from conventional methods?

This work aims to answer the above question. An AI control system is developed to manipulate a turbulent jet, one of the few best investigated and highly complicated classical flows, for maximized mixing. Six unsteady minijets are deployed as actuators. Following [3], genetic programming is chosen as a very powerful regression solver for the control law.

Experimental set-up

The round jet facility is schematically shown in figure 1, along with the assembly that produces up to 6 minijets. Details on the jet facility are given in [12]. The Reynolds number $Re_D = U_j D/\nu$ of the main jet is fixed at 8000, where U_j is the time-averaged centerline velocity measured at the nozzle exit, ν is the kinematic viscosity of air and D = 20 mm is the diameter of the nozzle, which is extended by a 47 mm long smooth tube of the same diameter. The coordinate system (x, y, z) is defined in figure 1(*a*, *b*), with its origin at the centre of the jet exit. The 6 unsteady radial minijets issued from orifices with a diameter of 1 mm are equidistantly placed at $x_i = -0.85D$, $y_i = (D/2)\cos\theta_i$, $z_i = (D/2)\sin\theta_i$, where $\theta_i = (i - 1)2\pi/6$, $i = 1,2, \ldots ,6$ (figure 1*b*, *c*). Their mass flow rate is determined by a flow-limiting valve and monitored by a mass flow meter, and the frequencies and duty cycles are independently controlled by individual electromagnetic valves that are operated in an ON/OFF mode. Figure 1(*d*) shows the arrangement of two hot-wire probes. The

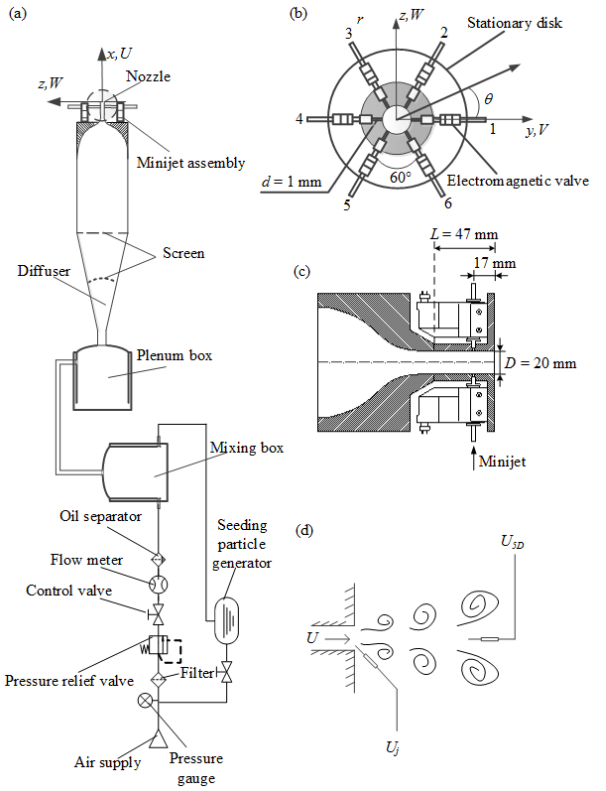

Figure 1: Sketch of the experimental setup: (a) main jet facility; (b) minijet arrangement; (c) minijet assembly; (d) hot-wire sensors.

jet exit velocity at $(x, y, z) = (0, D/4, 0)$ is measured with a tungsten wire of 5 µm in diameter, operated on a constant temperature circuit (Dantec Streamline) at an overheat ratio of 0.6. The centreline jet velocity at $x = 5D$ is monitored with a second hot-wire placed at $(x, y, z) = (5D, 0, 0)$ and the time-averaged velocity at this position is denoted by U_{5D}. Both hot-wires are calibrated at the jet exit using a pitot static tube connected to a micromanometer (Furness Controls FCO510). The cutoff and sampling frequencies are 500 Hz and 1 kHz, respectively. A planar high-speed particle image velocimetry (PIV) system, including a high speed camera (Dantec Speed Sence90C10, 2056×2056 pixels resolution) and a pulsed laser source (Litron LDY304-PIV, Nd:YLF, 120 mJ/pulse), is deployed for flow visualization in the *xz*, *xy* and *yz* planes. An oil droplet generator (TSI MCM-30) is used to generate, from olive oil, a fog with an average particle size of 1µm for seeding the flow.

Artificial intelligence control system

The AI control system is sketched in figure 2. Generally, a control system (solid line inside) facilitates a control goal for a plant (yellow) by control hardware and a control logic/ controller (red). The control hardware includes sensors (green) and actuators (blue), discussed above, which monitor the plant output (velocity signals) and execute instructions from the controller, respectively. The open-loop arrangement is shown in figure 1(*d*) for computing the cost value $J = U_{5D}/U_j$. The minimized J corresponds to the maximized decay rate $K = 1\text{-}J$ of jet centreline mean velocity, which is an indicator of the mixing efficacy of the jet [9].

The six-dimensional vector $\boldsymbol{b} = [b_1, b_2, \ldots, b_6]\dagger$ comprises all actuation commands: The *i*th minijet blows if the actuation command b_i is positive and is closed otherwise. Following [12], we search for a control law including multi-frequency forcing contained in $\boldsymbol{h} = [h_1, h_2 \ldots, h_6]\dagger$ ($h_i = \sin(\omega_e t - \phi_i)$, $i = 1,2, \ldots,$ 6, where t is time, ω_e is a reference frequency and ϕ_i is an initial phase). Then,

$$\boldsymbol{b} = \boldsymbol{K}(\boldsymbol{h}). \quad (1)$$

The non-linear function $\boldsymbol{K}$ can create arbitrary phase, higher harmonics, e.g. $1\text{-}2h_1^2 = \cos(2\omega_e t)$ as well as arbitrary sum and different frequencies. The control optimization searches for a law of form "equation (1)" which minimizes the cost, $\boldsymbol{K}^\star = \text{argmin}\, J[\boldsymbol{K}]$.

The regression problem implies the search for a mapping from a multiple input to a multiple output signal. Even in case of a linear function this implies the optimization of a great number of parameters, as exemplified above. We employ the powerful linear genetic programming as a regression solver and take the same parameters for the genetic operations as previous work [12]. The first generation of LGP, $n = 1$, contains $N_i = 100$ random control laws, also called individuals. Each individual is tested for 5 seconds in the experiment to yield the measured cost J_i^1. Subsequent generations are generated from the previous ones with genetic operations (elitism, crossover, mutation and replication) and tested analogously. After the in situ performance measurements, the individuals are re-numbered in order of performance, $J_1^n \leq J_2^n \leq \ldots \leq J_{Ni}^n$, where the superscript 'n' represents the generation number. As a plant specific rule, we discard and replace any individual for testing if one or more actuators are not active.

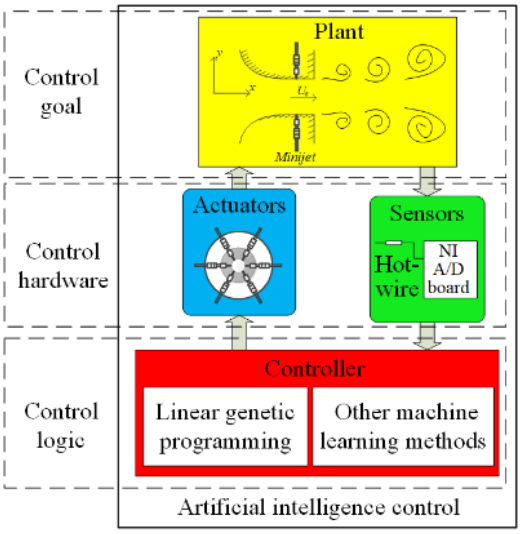

Figure 2: Principle sketch of the artificial intelligence control system

Results and discussion

Mass flow ratio and frequency

Our earlier studies to optimize the turbulent jet mixing for the same cost function and under the same conditions have identified the optimal $f_e = 67$ Hz for single-minijet forcing [12] and the optimal mass flow ratio $C_m = m_{mini}/m_j = 1.2\%$ [13], where m_j is the mass flow rate of the main jet.

Benchmarks from conventional open-loop control

The cost J_u of the unforced jet is 0.947 (figure 3), that is, $K \approx 0.05$; the typical flow visualization photograph shows the familiar jet flow structure in the *xy*-plane (figure 3a), as presented in [14]. Consider three actuations:

axisymmetric forcing $b_i = h_1\text{-}\alpha_a$, $i = 1, \ldots, 6$; (2a)

helical forcing $b_i = h_i\text{-}\alpha_h$, $i = 1, \ldots, 6$; (2b)

flapping forcing $b_i = h_i\text{-}\alpha_f$, $i = 1, \ldots, 6$. (2c)

Constants α_a, α_h and α_f characterize the duty cycles and have been optimized with respect to the cost. The costs $J_a = 0.665$, $J_h = 0.568$, $J_f = 0.423$ of the optimized axisymmetric, helical and flapping forcings, achieved from conventional open-loop control, provide the benchmarks for the AI control performance and are discussed in the next subsection.

AI control

The optimal AI control laws can always be cast in form of "equation (1)". Hence, we restrict the discussion to this periodic actuation. In figure 3, the square symbol marks the first and best individual, out of $N_i = 100$, of each generation. The remaining costs of each generation grow monotonously with the index. Every curve has a unique colour. The learning curve of AI control exhibits remarkable results, presented below, from generation n =1 to 30.

The best individual of the first generation or stage 1 has an axisymmetric control law $b_1 = b_2 = b_3 = b_4 = b_5 = b_6 = -0.832+\sin(\omega t + 4/6\pi)$ which determines excitation frequency f_e and duty cycle α of each minijet is $0.5f_0$ and 13.3%, respectively. This law is equivalent to "equation (2a)" except a time shift. Figure 3(*b*) and figure 4(*a*1-*a*6) illustrate the typical flow structures in the *xy*-plane and *yz*-plane of $x/D = 0.25$, respectively. The flow structure in the *xy*-plane exhibits an appreciably larger lateral spread than the unforced jet. The flow images in the cross-sectional plane are captured at a sampling rate of 405 Hz, corresponding to 3 f_0 and 6 f_e. The six consecutive times in figure 4(*a*1-*a*6) represent one actuation period. Figure 4(*a*1, *a*2) displays largely the full-moon-like structure, corresponding to the braid region and the ring vortex, respectively. Each injecting unsteady minijet induces one pair of streamwise vortices, which interact with the mushroom-like structures generated due to the perturbed braid instability, resulting in greatly accelerated jet entrainment and spread [14]. Obviously, mushroom-like structures remain axisymmetric for different phases. The performance $J_1^1 = 0.626$ (see figure 3) is slightly better than the benchmark of axisymmetric forcing. The reason may be attributed to the converged 60-sec. velocity data acquisition to calculate J_a as compared to the 5-sec. and less accurate measurement of AI control.

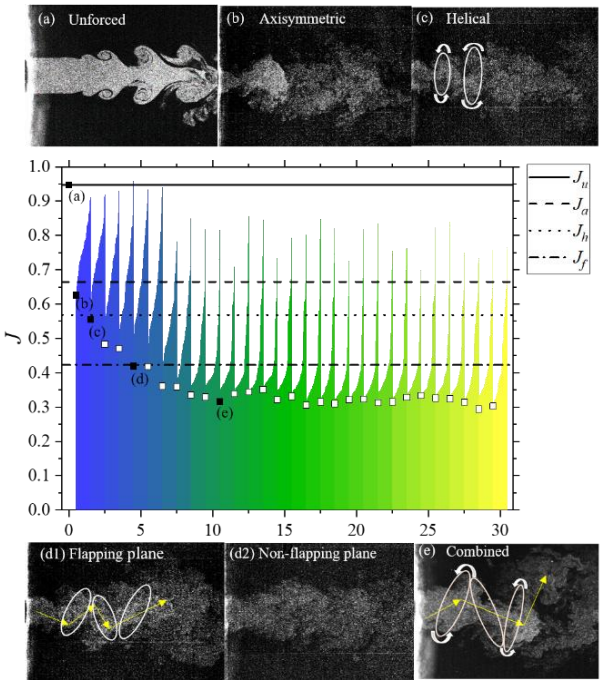

Figure 3: The learning curve of AI control and representative flow structures. J_u, J_a, J_h and J_f are costs corresponding to the benchmarks of unforced, open-loop axisymmetric, helical and flapping forcings, respectively.

Stage 2 starts with the second generation when AI control discovers a better performing helical forcing which clearly shows a uniformly traveling wave in the azimuthal direction, its cost being slightly lower than J_h. The flow appears rotating, as indicated by the crooked arrows in figure 3(*c*). This rotational motion is evident in the flow images captured in the cross-sectional plane of $x/D = 0.25$ (figure 4*b*1-*b*6), which show the clockwise rotating ring structure generated from the minijet-induced early rollup [9]. Helical forcing reduces J further as expected from the numerical simulation study of a similar jet mixing optimization [5]. Local spatial stability analysis indicates that helical perturbations, unlike axisymmetric forcing, are spatially amplified downstream of the potential core [4].

Stage 3 is characterized by flapping forcing $b_1 = b_2 = b_3 = -0.811 + \sin(\omega t + 2/6\,\pi)$ and, $b_4 = b_5 = b_6 = -0.782 - \sin(\omega t + 2/6\pi)$, which occurs from the fifth generation. An optimized anti-phase yields a reproducibly better mixing. As shown in figure 3(*d*1) the jet column wobbles up and down in the flapping plane but not in the orthogonal plane (figure 3*d*2); as a result, the flow images in the *yz*-plane (figure 4*c*1-*c*6) shows either part of the ring vortex (*c*3, *c*6) or counter-rotating mushroom-like structures (*c*1-*c*2, *c*4-*c*5) generated in the braid region, as [15] observed. The incomplete ring structure on the left (*c*3) or right (*c*6) side of the core occurs every half period due to anti-phase flapping forcing.

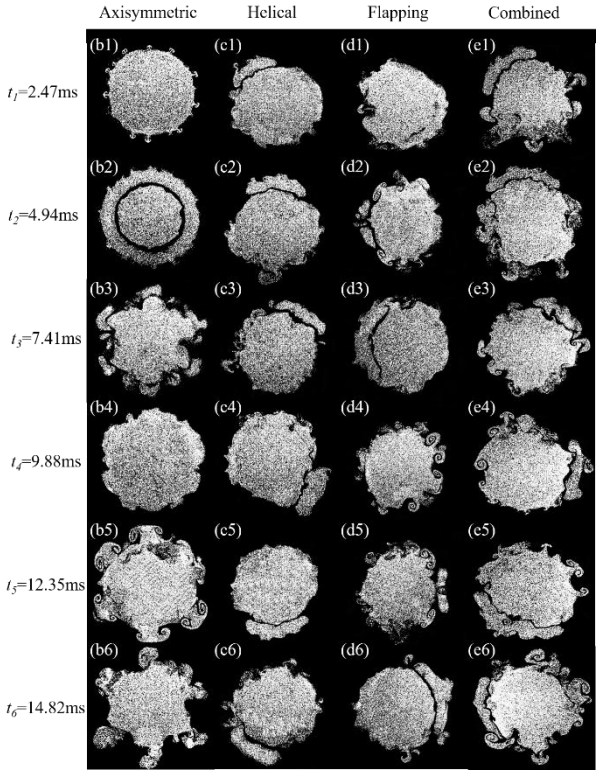

Figure 4: Sequential photographs of the cross-sectional flow structure at $x/D = 0.25$ for the four stages: (*b*1-*b*6) axisymmetric forcing, (*c*1-*c*6) helical forcing, (*d*1-*d*6) flapping forcing, and (*e*1-*e*6) combined forcing.

The eleventh generation marks the emergence of stage 4; AI control discovered a surprising combination of asymmetric flapping forcing and helical forcings along with the generation of longitudinal mushroom structures, where the flow structure is characterized by the asymmetry (the footprint of flapping motion), rotating satellite structure and mushroom-like structures at all phases. The combined forcing significantly

outperforms the flapping forcing found in generation 5 with appreciably more lateral spread in all directions and the corresponding J plunging to less than 1/3 of the unforced jet. The flow structure (figure 3*e*) exhibits the features of not only flapping jet column, similar to figure 3(*d*), but also rotational motion, as is evident in figure 4(*d*1-*d*6). The cost and actuation mechanism hardly change in following generations, pointing to the convergence of the AI learning process. This actuation mechanism is reproducible, that is, the combined flapping and helical forcings and approximately the same converged cost have been observed in all experiments, notwithstanding a change in the initial parameters of the first generation.

Conclusions

An AI control system has been developed, which learns automatically how to manipulate a spatially distributed actuation and thus a turbulent jet for the targeted cost. Like virtually all control strategies of nonlinear dynamics, AI control solutions do not come with a proof of global optimality. Yet, the results for jet mixing optimization demonstrate a number of highly desirable features. First, AI control has unveiled a few typical control laws or forcings, i.e., axisymmetric, helical and flapping, in its learning process and eventually converged to a sophisticated spatio-temporal actuation which is the combination of the individual forcings. This combination has produced a fascinating turbulent flow structure characterized by rotating and flapping jet column, along with the generation of mushroom like structures, all acting to enhance jet mixing and thus vastly outperforming several known optimal benchmark forcings. Note that the learning time of 3000 individuals or 6 hours wind-tunnel testing is remarkably short for such a complicated solution. Second, unlike other simple conventional open or closed-loop control methods, AI control could find optimal control laws without too much prior flow physics. Third, the cost J corresponding to AI-learned combination is reproducible with other initial generations. The control laws may analytically differ but produce almost identical actuation commands. Fourth, the parameters of the underlying genetic programming are taken verbatim from [3] and were already proven useful in many other experiments. No sensitive dependence on the parameters has been observed so far and AI control can be expected to yield near-optimal results in its first application to a new plant. Finally, the search space for a control law is extremely large and of very high dimensions, including multiple frequencies, minijet configurations, temporal and spatial phase differences between the configurations, and duty cycles of minijets, along with sensor feedback.

Acknowledgments

Yu Zhou wishes to acknowledge support given to him from NSFC through grants 11632006 and U1613226 and from Research Grants Council of Shenzhen Government through grants JCYJ20160531193220561 and JCY20160531192108351.

Bernd R. Noack acknowledges funding from the French National Research Agency (ANR) under Grants “iCODE”, “ACTIV_ROAD” and “FlowCon”, from LIMSI and from Paris Saclay (SMEMaG).

References

[1] Akervik, E., Hoepffner, J., Ehrenstein, U. and Henningson, D. S., Optimal growth, model reduction and control in a separated boundary-layer flow using global eigenmodes, *J. Fluid Mech.*, **579**, 2007, 305–314.

[2] Becker, R., King, R., Petz, R. and Nitsche, W., Adaptive closed-loop separation control on a high-lift configuration using extremum seeking, *AIAA J.*, **45**, 2007, 1382-1392.

[3] Duriez, T., Brunton, S. L. and Noack, B. R., Machine Learning Control — Taming Nonlinear Dynamics and Turbulence, volume 116 of Fluid Mechanics and Its Applications, Springer-Verlag, 2016.

[4] Garnaud, X., Lesshafft, L., Schmid, P. J. and Huerre, P., The preferred mode of incompressible jets: linear frequency response analysis, J. Fluid Mech., **716**, 2013, 189–202.

[5] Hilgers, A. and Boersma, B. J., Optimization of turbulent jet mixing, *Fluid Dyn. Res.*, **29**, 2001, 345–368.

[6] Koumoutsakos, P., Freund, J. and Parekh, D., Evolution strategies for automatic optimization of jet mixing, *AIAA J.*, **39**, 2001, 967–969.

[7] Moin, P. and Bewley, T., Feedback control of turbulence, *Annual Review of Fluid Mechanics*, 1994, **47**.

[8] Onofrio, S., Shervin, B., Luca, B. and Henningson, D. S., Feedback control of three-dimensional optimal disturbances using reduced-order models, *J. Fluid Mech.*, **677**, 2011, 63–102.

[9] Perumal, A. K. and Zhou, Y., Parametric study and scaling of jet manipulation using an unsteady minijet, *J. Fluid Mech.*, **848**, 2018, 592–630.

[10] Rechenberg, I., *Evolutionsstrategie: Optimierung technischer Systeme nach Prinzipien der biologischen Evolution*, Frommann-Holzboog, Stuttgart, 1973.

[11] Sipp, D., Marquet, O., Meliga, P. and Barbagallo, A., Dynamics and control of global instabilities in open-flows: A linearized approach, *Appl Mech Rev.*, **63**, 2010, 030801.

[12] Wu, Z., Fan, D., Zhou, Y., Li, R. and Noack, B. R., Jet mixing optimization using machine learning control., Exp. Fluids, **59**, 2018, 131.

[13] Wu, Z., Wong, C. W. and Zhou, Y., Dual-input/single-output extremum-seeking system for jet control, *AIAA J.*, **56**, 2018, 1463–1471.

[14] Yang, H. and Zhou, Y., Axisymmetric jet manipulated using two unsteady minijets, *J. Fluid Mech.*, **808**, 2016, 362–396.

[15] Yang, H., Zhou, Y., So, R. M. and Liu, Y., Turbulent jet manipulation using two unsteady azimuthally separated radial minijets, *Proceedings of the Royal Society A Mathematical Physical & Engineering Sciences*, **472**, 2016, 20160417.

[16] Zhang, M. M., Cheng, L. and Zhou, Y., Closed-loop controlled vortex shedding and vibration of a flexibly supported square cylinder under different schemes, *Phys Fluids*, **16**, 2004, 1439–1448.